Laboratoire d'Annecy de Physique des Particules

Measurements and interpretations of STXS, differential and fiducial cross sections in Higgs boson decays to two photons with the ATLAS detector

Eleonora Rossi

on behalf of the ATLAS Collaboration

EPS-HEP2021, 26/07/2021

The enigma of mass

Higgs-boson properties: precision measurements

Two complementary measurements used to explore the properties of the Higgs boson:

Fiducial cross sections:

- largely model-independent measurements.
- Include information on the decay.
- Different distributions can be measured.
- Fiducial selection matches experimental selection (reduce full phase space extrapolation).

[LHCHWGFiducialAndSTXS]

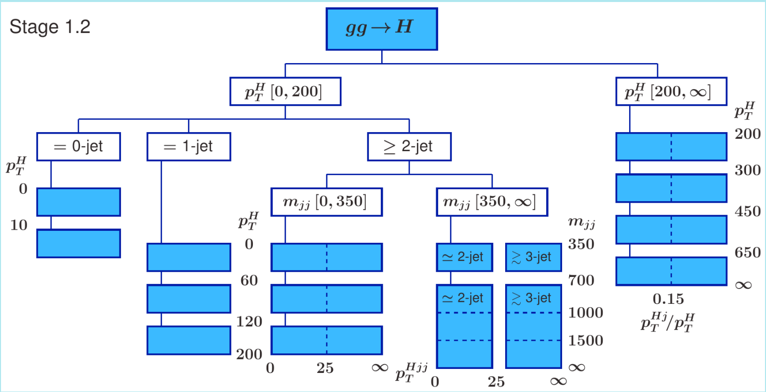

Simplified template cross section (STXS):

- STXS targets phase space regions within production modes, using Standard Model kinematics as a template.
- Categorise each production mode in bins of key (truth) quantities (p_T^H, N_{jets}, m_{jj}, …).
- Reduce theory systematics, but more model-dependent.
- No decay information available in STXS (for the moment).

LAPP Higgs cross sections in $H \to \gamma\gamma$ decay channel

ATLAS-CONF-2019-029

- Fiducial integrated and differential cross sections (2015–2018 dataset, $\sqrt{s} = 13$ TeV - 139 fb^{-1}):
  - ✦ integrated cross section: $\sigma \times BR = N_{signal}/(L \cdot \epsilon \cdot A)$ -> backup
  - ✦ differential cross section: $d(\sigma \times BR)/dx,\ x = p_T^{\gamma\gamma}, |y_{\gamma\gamma}|, N_{jets}, p_T^{j1}, m_{jj}, \Delta\varphi_{jj}$ -> interpretations.

  Observables sensitive to new physics, spin and CP-quantum number of the Higgs ($\Delta\varphi_{jj}$) but also QCD calculations in the SM ($p_T^{\gamma\gamma}, p_T^{j1}, N_{jets}$).
- Main improvements with respect to previous measurements:
  - ✦ reduced statistical and systematic uncertainties;
  - ✦ improved signal efficiency / background rejection for diphotons.

ATLAS-CONF-2020-026

- STXS cross sections (2015–2018 dataset, $\sqrt{s} = 13$ TeV - 139 fb^{-1}):
  - ✦ measure production cross sections in the STXS framework -> Higgs-boson production phase space ($|y_H| < 2.5$) split by production process as well as kinematic and event properties.
- Main improvements with respect to previous measurements:
  - ✦ increased granularity (including differential $t\bar{t}H$ measurement)-> 27 STXS regions
  - ✦ new categorisation; reduces uncertainties and correlations.

The $H \to \gamma\gamma$ analysis in a nutshell

- Small BR (~0.2%) but excellent performance of photon reconstruction and identification + mass resolution-> clean signature.
- Experimental signature:
  - ✦ narrow resonance with a width consistent with detector resolution rising above a smooth background in the diphoton invariant mass ($m_{\gamma\gamma}$) distribution.

Analysis cuts

- ✦ defined by two isolated photons with $p_T^{leading}/m_{\gamma\gamma} > 0.35$ and $p_T^{subleading}/m_{\gamma\gamma} > 0.25$.
- ✦ $|\eta| < 1.37$ or $1.52 < |\eta| < 2.37$.
- ✦ jets: $p_T > 30$ GeV and rapidity $|y| < 4.4$.
- ✦ $|y_H| < 2.5$ for STXS measurements.

- Results: fit diphoton mass $m_{\gamma\gamma}$ using parameterised signal and background shapes in each category.

ATLAS-CONF-2020-026

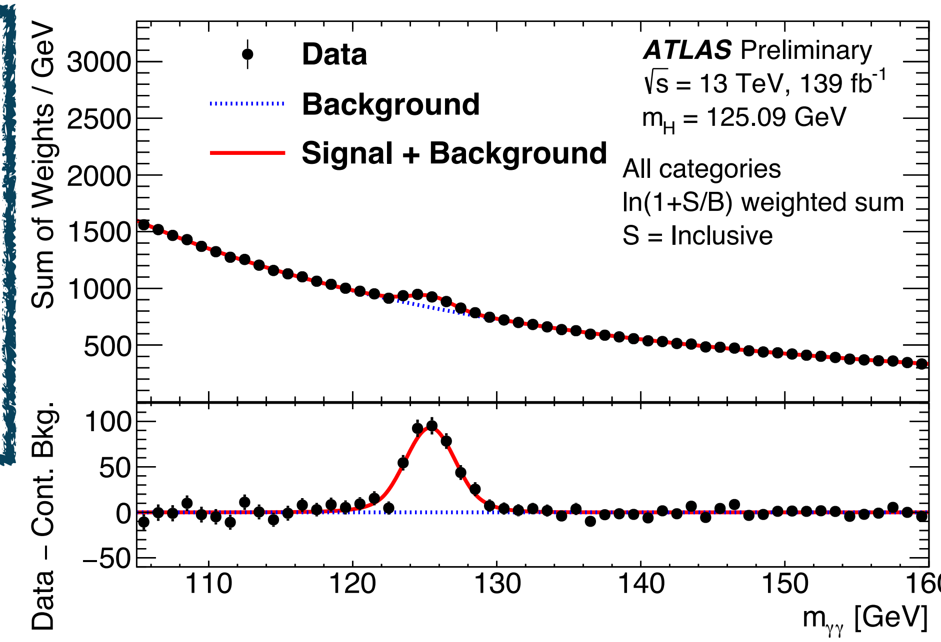

Categorisation for STXS measurements

- Multi-classifier BDT used to separate events into STXS bins.
- Binary BDT classifier applied in each STXS bin to divide events into different categories and improve the sensitivity.

Training variables in backup

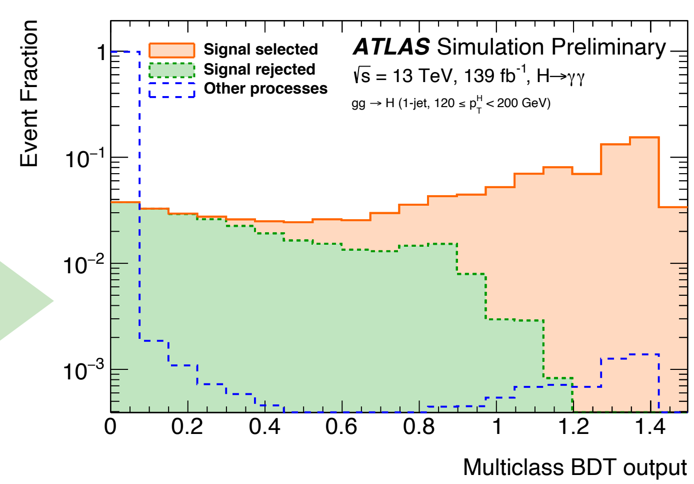

ATLAS-CONF-2020-026

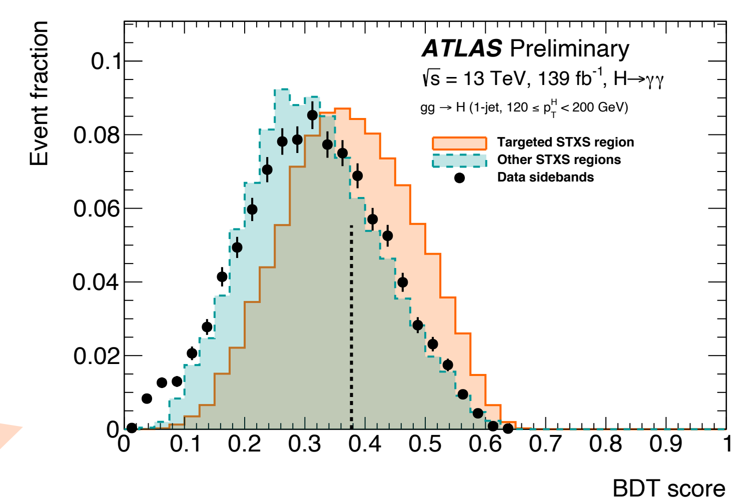

The $H \to \gamma\gamma$ analysis in a nutshell

- Small BR (~0.2%) but excellent performance of photon reconstruction and identification + mass resolution-> clean signature.
- Experimental signature:
  - ✦ narrow resonance with a width consistent with detector resolution rising above a smooth background in the diphoton invariant mass ($m_{\gamma\gamma}$) distribution.

Analysis cuts

- ✦ defined by two isolated photons with $p_T^{leading}/m_{\gamma\gamma} > 0.35$ and $p_T^{subleading}/m_{\gamma\gamma} > 0.25$.
- ✦ $|\eta| < 1.37$ or $1.52 < |\eta| < 2.37$.
- ✦ jets: $p_T > 30$ GeV and rapidity $|y| < 4.4$.
- ✦ $|y_H| < 2.5$ for STXS measurements.

ATLAS-CONF-2020-026

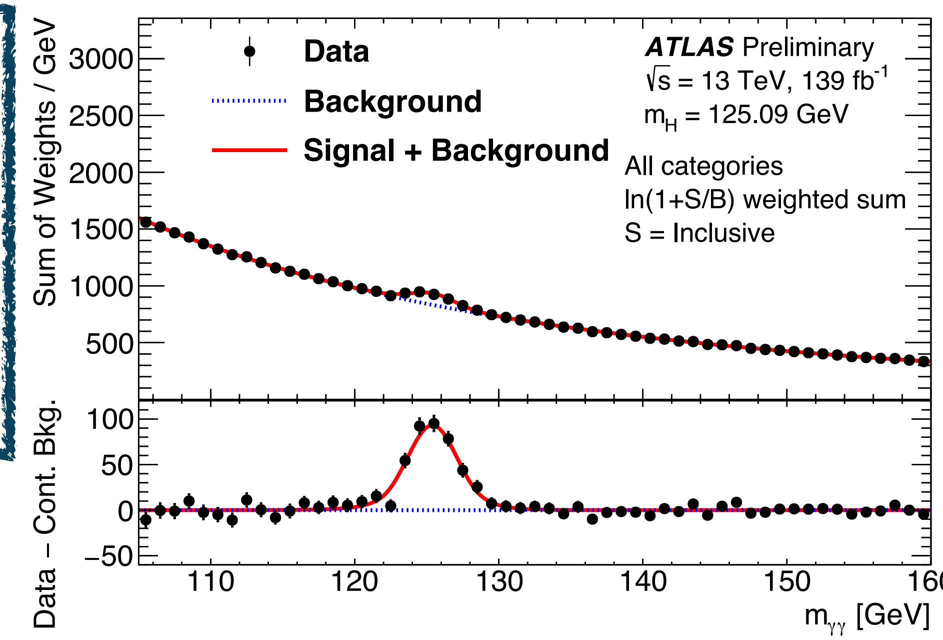

- Results: fit diphoton mass $m_{\gamma\gamma}$ using parameterised signal and background shapes in each category.

Unfolding for fiducial measurements

- The reconstruction-level data signal yields are unfolded to particle level using a bin-by-bin correction factor:

$$\sigma_{\text{fid}} = \frac{N^{\text{sig}}}{c_{\text{fid}}\mathcal{L}_{\text{int}}} \qquad \left(\frac{d\sigma}{dx}\right)_i = \frac{N_i^{\text{sig}}}{c_{\text{fid},i}\,\Delta x_i\,\mathcal{L}_{\text{int}}}$$

Bin-by-bin correction factor for detector efficiency and resolution effects.
Matrix-based unfolding as a check (full detector response matrix).

ATLAS-CONF-2019-029

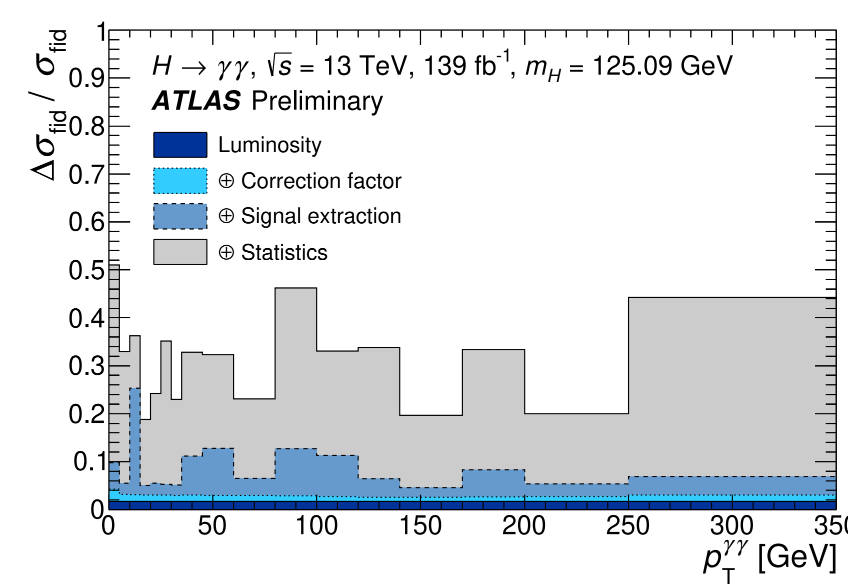

$H \to \gamma\gamma$: differential and fiducial cross sections

- The distributions are compared to the state-of-the art theory predictions and used for the interpretations.

- The $p_T^{\gamma\gamma}$ distribution is compared to NNLOJET+SCET.
- The $p_T^{\gamma\gamma}$ distribution reaches out to 350 GeV, a region where top-quark mass effects start to become sizeable.
- A finer binning has been chosen at lower $p_T^{\gamma\gamma}$ to probe the region where resummation effects are important and to probe the **charm quark Yukawa coupling** -> results presented in Marko's talk (+ **backup**).

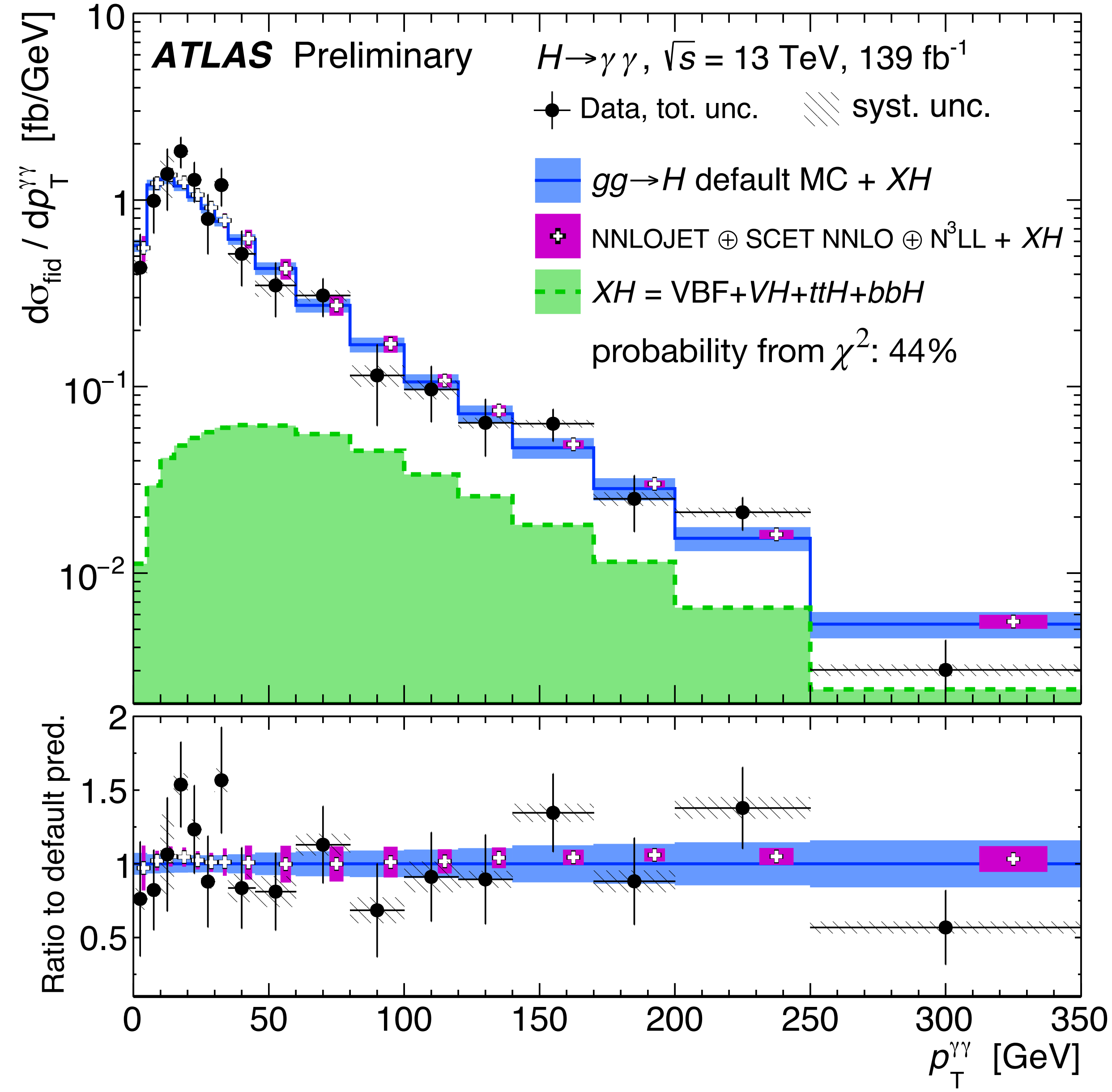

ATLAS-CONF-2019-029

$H \to \gamma\gamma$: differential and fiducial cross sections

- The distributions are compared to the state-of-the art theory predictions and used for the interpretations.

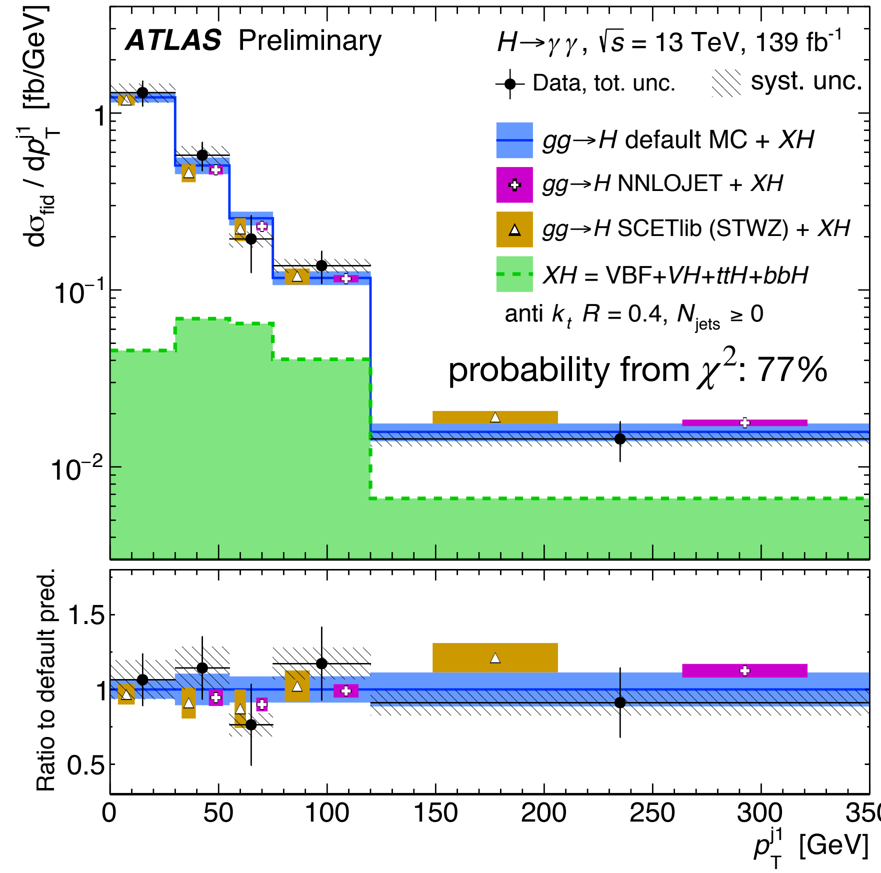

- Kinematics observables with sensitivity to new physics.
- $\Delta\phi_{jj}$: sensitive to CP properties of the Higgs boson.
- Good agreement observed w.r.t. SM predictions.

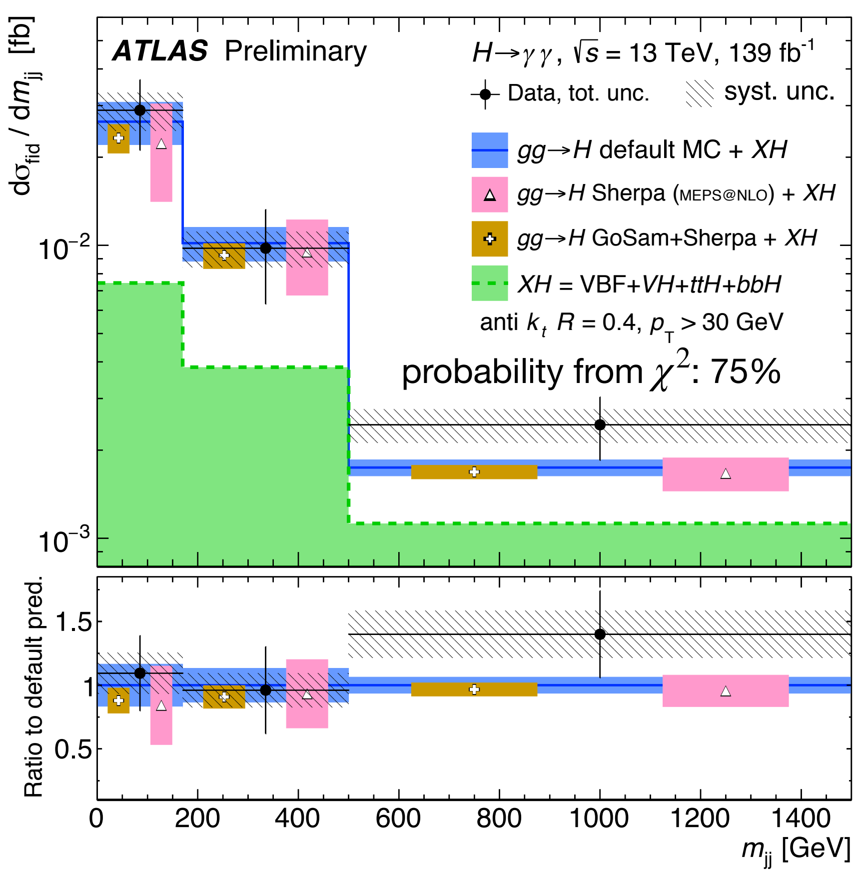

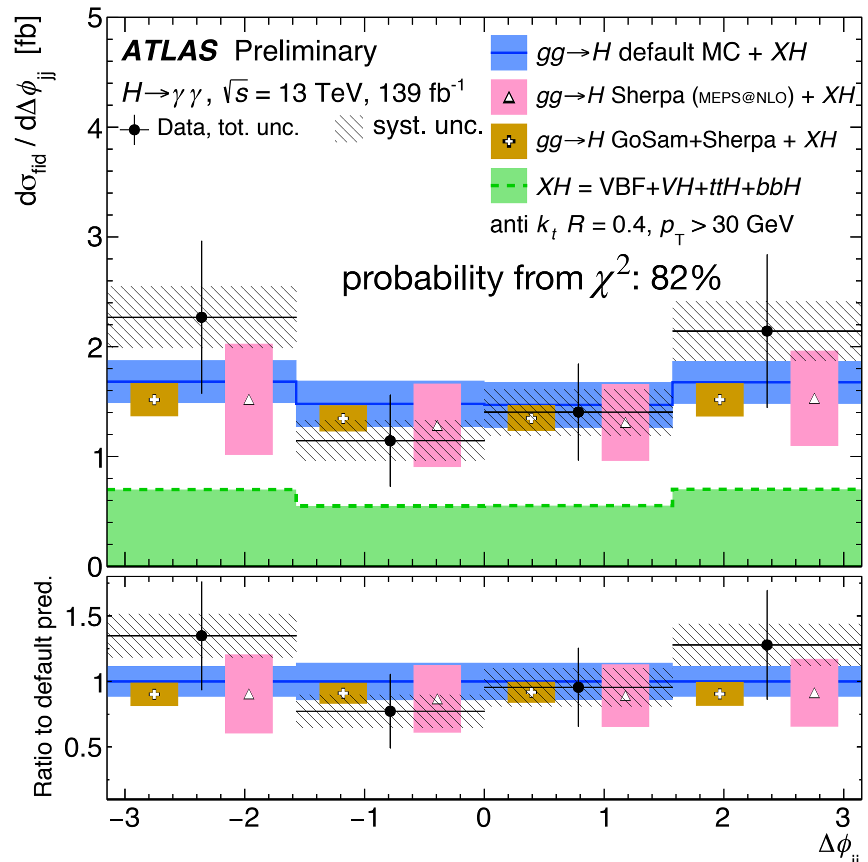

other interesting distributions in backup

ATLAS-CONF-2019-029

Anomalous Higgs-boson interactions through EFT

An effective field theory (EFT) approach can be used to interpret Higgs-boson interactions:

- additional CP-even and CP-odd interactions can change the event rates, the kinematic properties of the Higgs boson, etc.., from those predicted by the SM.

$$\mathscr{L}_{EFT} = \mathscr{L}_{SM} + \sum_{i,D} \frac{c_i^{(D)}}{\Lambda^{D-4}} \mathcal{O}_i^{(D)}$$

Wilson coefficients

- The differential $H \to \gamma\gamma$ cross sections are sensitive to operators that affect the Higgs-boson interactions with gauge bosons (5 differential distributions).

$$d(\sigma \times BR)/dx,\ x = p_T^{\gamma\gamma}, N_{jets}, p_T^{j1}, m_{jj}, \Delta\varphi_{jj}$$

- Two different EFT basis have been used:
  - ✦ the SILH basis of the Higgs Effective Lagrangian
  - ✦ the Warsaw basis of the SMEFT Lagrangian.

$$\mathcal{L}_{\text{eff}}^{\text{SILH}} \supset \bar{c}_g O_g + \bar{c}_\gamma O_\gamma + \bar{c}_{HW} O_{HW} + \bar{c}_{HB} O_{HB} + \tilde{c}_g \tilde{O}_g + \tilde{c}_\gamma \tilde{O}_\gamma + \tilde{c}_{HW} \tilde{O}_{HW} + \tilde{c}_{HB} \tilde{O}_{HB}$$

$$\mathcal{L}_{\text{eff}}^{\text{SMEFT}} \supset \bar{C}_{HG} O'_g + \bar{C}_{HW} O'_{HW} + \bar{C}_{HB} O'_{HB} + \bar{C}_{HWB} O'_{HWB} + \tilde{C}_{HG} \tilde{O}'_g + \tilde{C}_{HW} \tilde{O}'_{HW} + \tilde{C}_{HB} \tilde{O}'_{HB} + \tilde{C}_{HWB} \tilde{O}'_{HWB}$$

ATLAS-CONF-2019-029

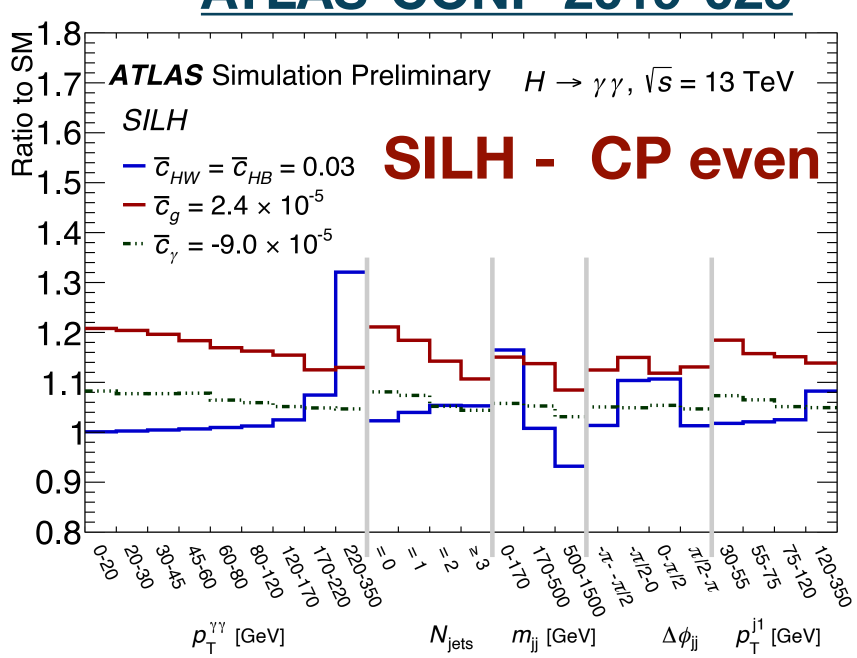

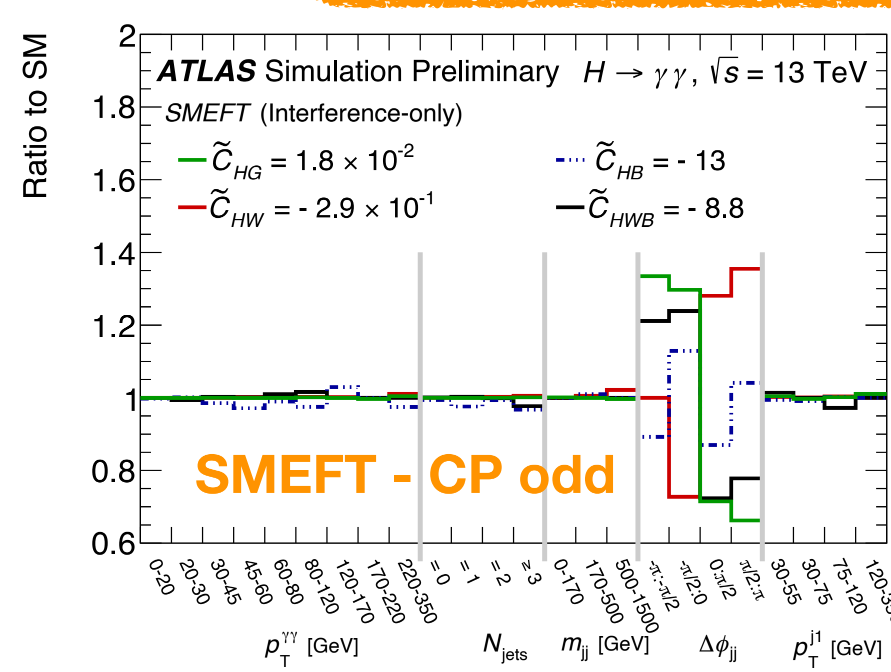

Plots including CP-odd (SILH) and CP-even (SMEFT) are in backup

Anomalous Higgs-boson interactions through EFT

- 1D and 2D limits obtained fitting one or two WC at the time (and fixing the others to 0 -> SM).

$$\mathcal{L}_{\rm eff}^{\rm SILH} \supset \quad \bar{c}_g O_g + \bar{c}_\gamma O_\gamma + \bar{c}_{HW} O_{HW} + \bar{c}_{HB} O_{HB} + \tilde{c}_g \tilde{O}_g + \tilde{c}_\gamma \tilde{O}_\gamma + \tilde{c}_{HW} \tilde{O}_{HW} + \tilde{c}_{HB} \tilde{O}_{HB}$$

- Destructive interference causes the ggF production cross section=0 around $\bar{c}_g \sim -2.2 \cdot 10^{-4}$ for $\tilde{c}_g \sim 0$-> structure seen in the observed limits in the two-dimensional parameter plane.

$$\mathcal{L}_{\rm eff}^{\rm SMEFT} \supset \quad \overline{C}_{HG} O'_g + \overline{C}_{HW} O'_{HW} + \overline{C}_{HB} O'_{HB} + \overline{C}_{HWB} O'_{HWB} + \widetilde{C}_{HG} \widetilde{O}'_g + \widetilde{C}_{HW} \widetilde{O}'_{HW} + \widetilde{C}_{HB} \widetilde{O}'_{HB} + \widetilde{C}_{HWB} \widetilde{O}'_{HWB}$$

- The limits in the interference and interference + pure BSM cases are very similar for coefficients of CP-even operators (interference terms dominate).
- Significant differences emerge for the CP-odd ones for which the interference term is vanishing (for inclusive observables).

ATLAS-CONF-2019-029

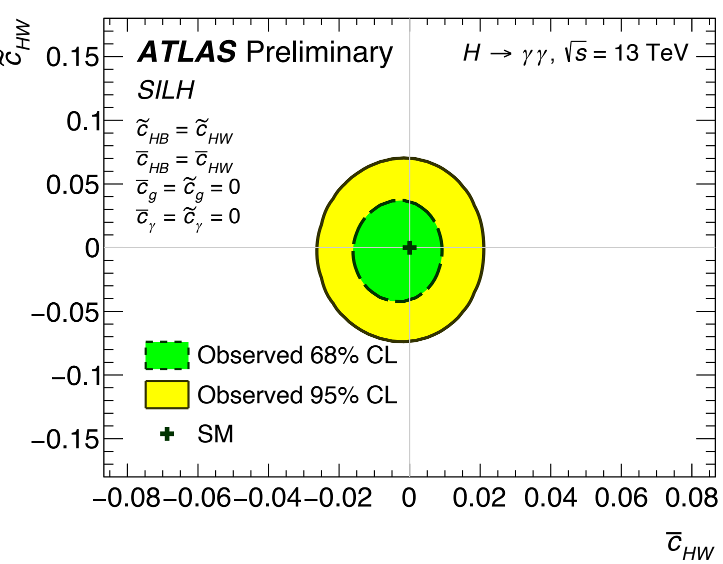

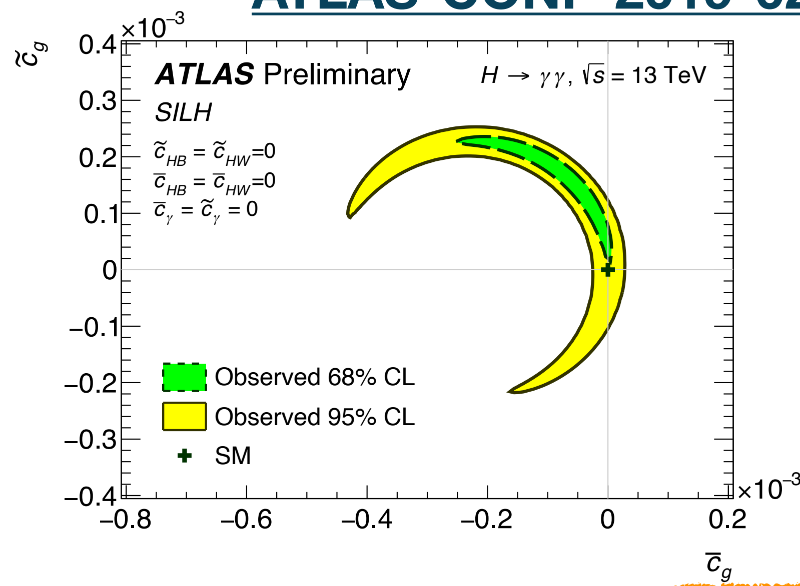

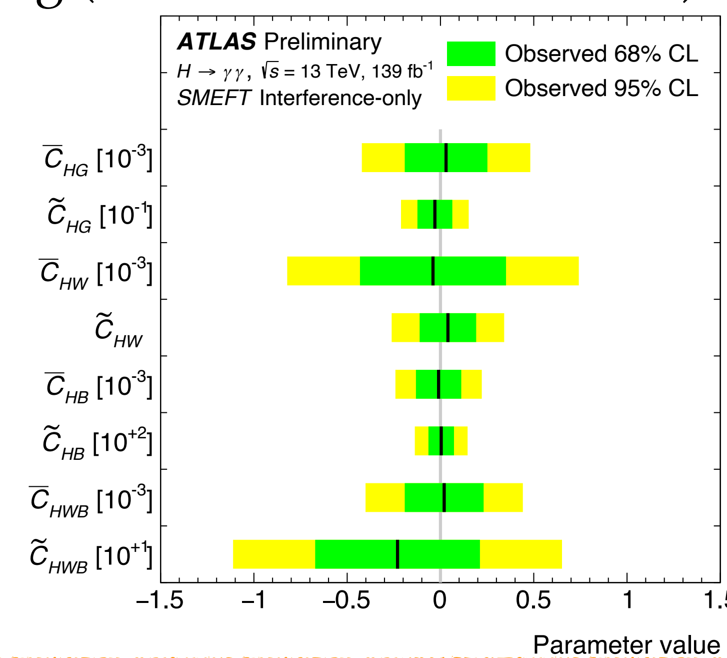

Coefficient	Observed 95% CL limit	Expected 95% CL limit
$\bar{c}_g$	$[-0.26, 0.26] \times 10^{-4}$	$[-0.25, 0.25] \cup [-4.7, -4.3] \times 10^{-4}$
$\tilde{c}_g$	$[-1.3, 1.1] \times 10^{-4}$	$[-1.1, 1.1] \times 10^{-4}$
$\bar{c}_{HW}$	$[-2.5, 2.2] \times 10^{-2}$	$[-3.0, 3.0] \times 10^{-2}$
$\tilde{c}_{HW}$	$[-6.5, 6.3] \times 10^{-2}$	$[-7.0, 7.0] \times 10^{-2}$
$\bar{c}_\gamma$	$[-1.1, 1.1] \times 10^{-4}$	$[-1.0, 1.2] \times 10^{-4}$
$\tilde{c}_\gamma$	$[-2.8, 4.3] \times 10^{-4}$	$[-2.9, 3.8] \times 10^{-4}$

Coefficient	95% CL, interference-only terms	95% CL, interference and quadratic terms
$\overline{C}_{HG}$	$[-4.2, 4.8] \times 10^{-4}$	$[-6.1, 4.7] \times 10^{-4}$
$\widetilde{C}_{HG}$	$[-2.1, 1.6] \times 10^{-2}$	$[-1.5, 1.4] \times 10^{-3}$
$\overline{C}_{HW}$	$[-8, 2, 7.4] \times 10^{-4}$	$[-8.3, 8.3] \times 10^{-4}$
$\widetilde{C}_{HW}$	$[-0.26, 0.33]$	$[-3.7, 3.7] \times 10^{-3}$
$\overline{C}_{HB}$	$[-2.4, 2.3] \times 10^{-4}$	$[-2.4, 2.4] \times 10^{-4}$
$\widetilde{C}_{HB}$	$[-13.0, 14.0]$	$[-1.2, 1.1] \times 10^{-3}$
$\overline{C}_{HWB}$	$[-4.0, 4.4] \times 10^{-4}$	$[-4.2, 4.2] \times 10^{-4}$
$\widetilde{C}_{HWB}$	$[-11.1, 6.5]$	$[-2.0, 2.0] \times 10^{-3}$

$H \to \gamma\gamma$: STXS cross sections

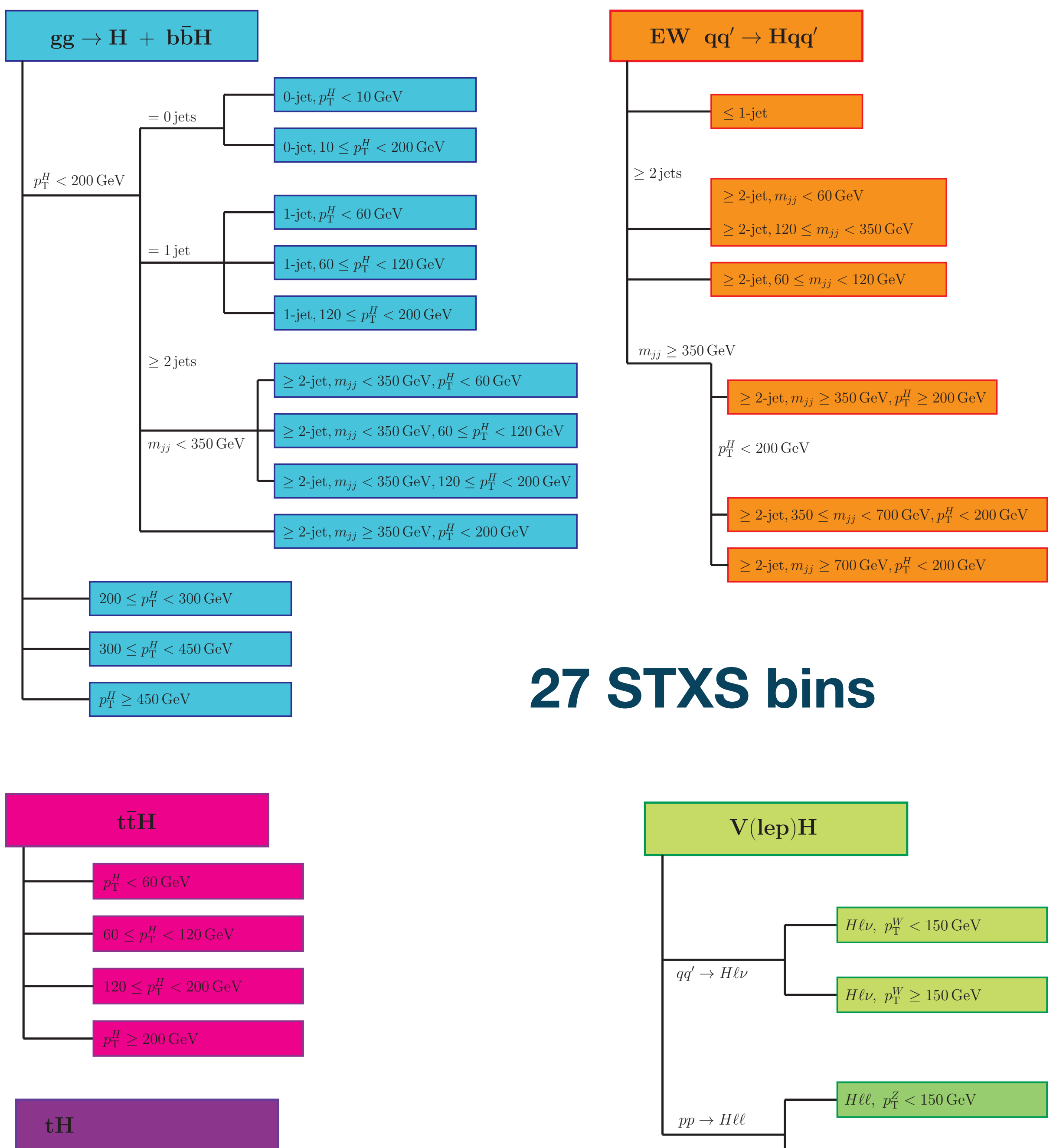

27 STXS bins

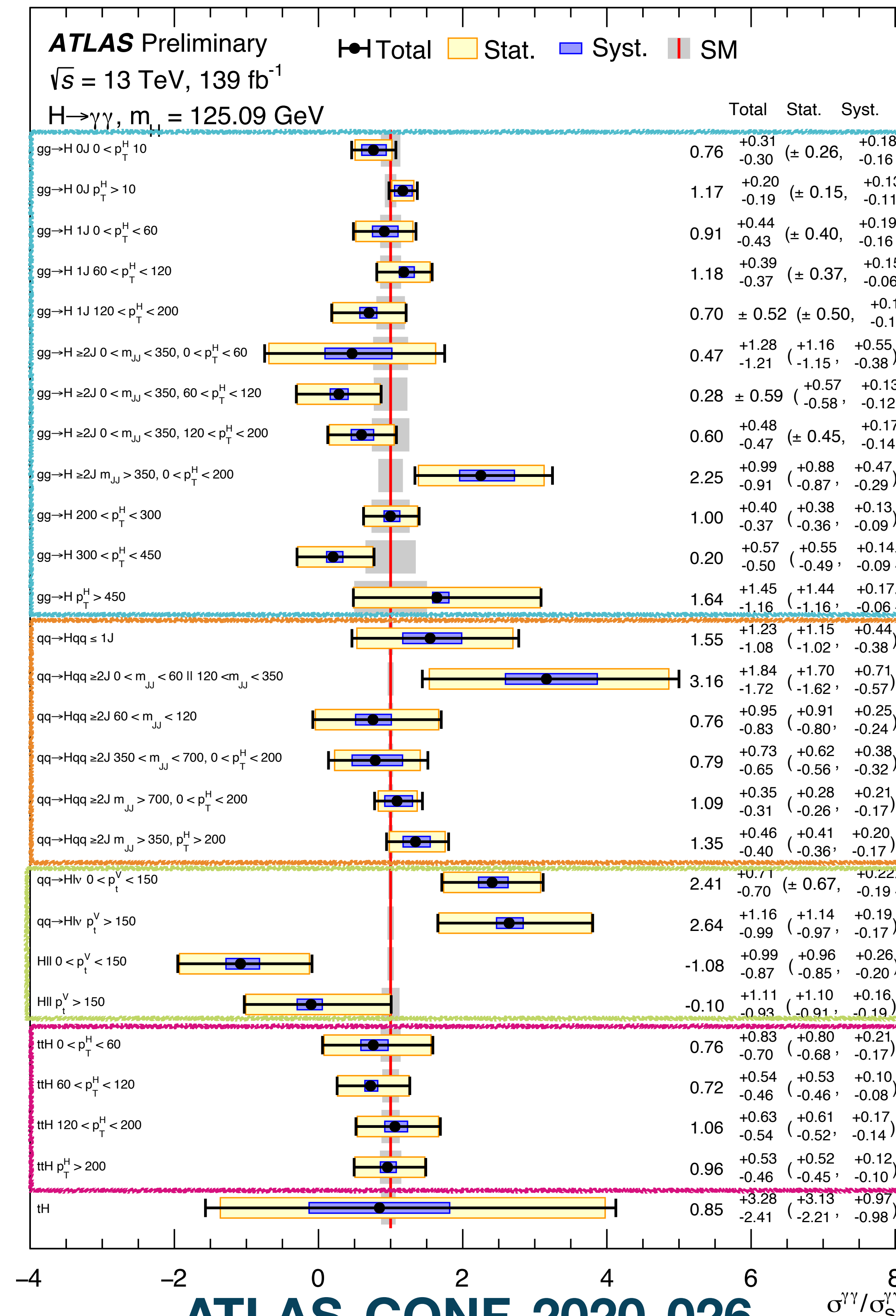

- The relative uncertainties on the measurements range from 20% to more than 100%.

ATLAS-CONF-2020-026

$H \to \gamma\gamma$: STXS cross sections

- Large uncertainties occur in particular in regions of high p_T^H and p_T^V, as well as the low-m_{jj} regions of $qq' \to Hqq'$.
- The systematic component of uncertainties is smaller than the statistical component (similar values for the 0-jet regions of $gg \to H$).
- No significant deviations from the SM expectation are observed-> compatibility between the measurements and the SM predictions corresponds to a p-value of 60%.

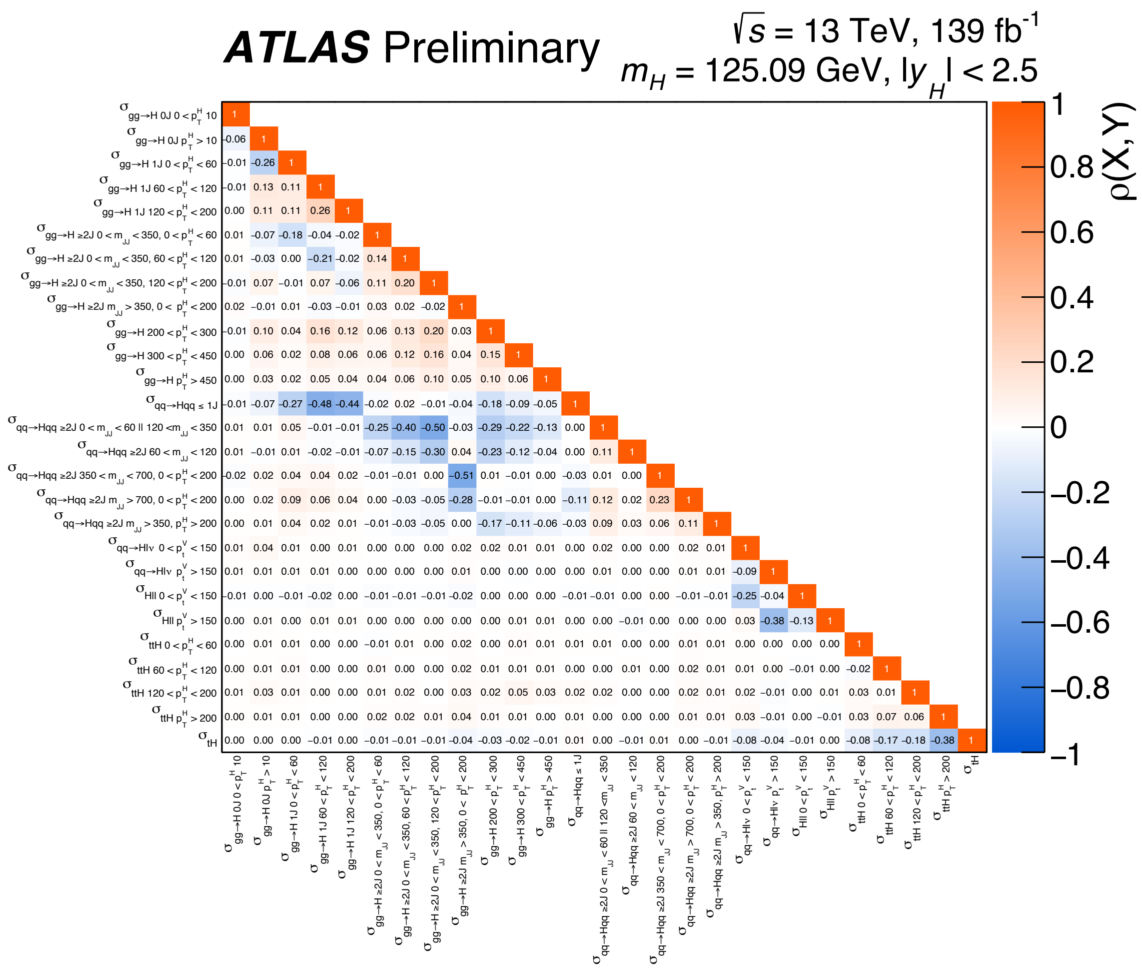

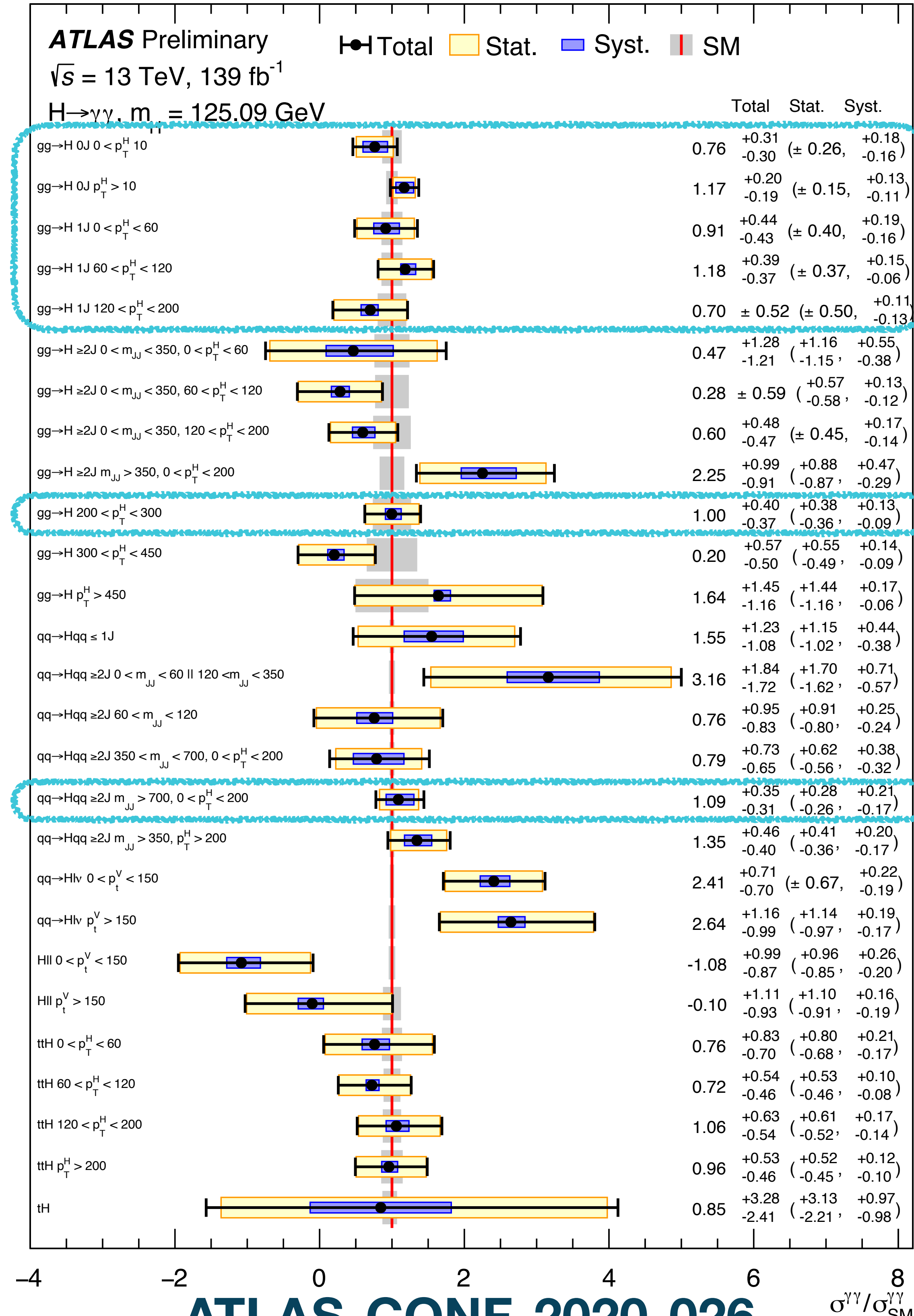

ATLAS-CONF-2020-026

- An upper limit of ~8x SM prediction on tH production.

Conclusion

- Two complementary approaches exploited to measure the Higgs cross sections in diphoton decay channel:
  - all results in agreement with the SM predictions;
  - interpretations provided in the context of EFT theories for fiducial differential results;
  - differential cross-section as a function $p_T^{\gamma\gamma}$ used to probe the charm Yukawa coupling of the Higgs boson.

  - STXS cross-sections in 27 regions of Higgs boson production phase space;
  - STXS: upper limit of ~8x SM prediction on tH production.

- Still room to improve full Run 2 results -> results for both fiducial differential and STXS measurement **coming soon** (including EFT and kappa interpretations).

Thank you for your attention

$H \to \gamma\gamma$: differential and fiducial cross sections

- The distributions are compared to the state-of-the art theory predictions and used for the interpretations.

- Comparisons in exclusive and inclusive bins.
- Agreement is observed between the measured N_{jets} distributions and all predictions with precision better than NLO (N³LO normalisation improves the agreement).
- Systematic uncertainties having the largest impact (6%-25%) are the jet energy scale and resolution.

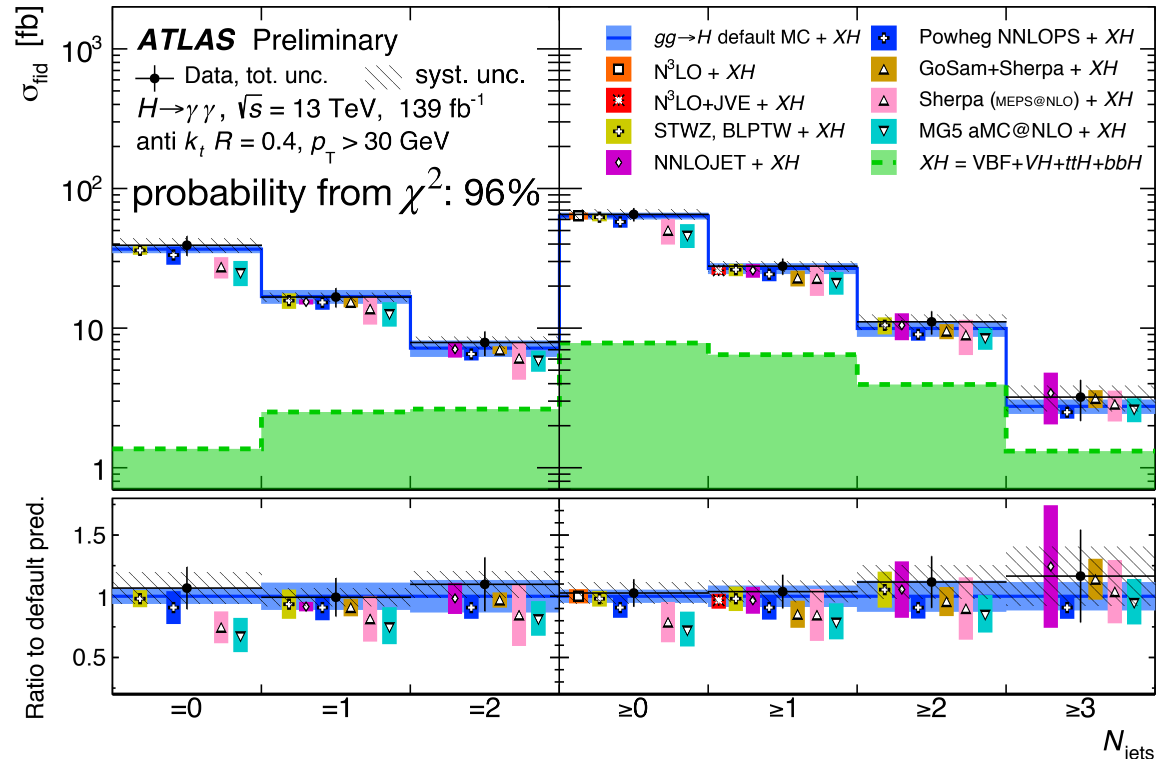

- The $|y_{\gamma\gamma}|$ distribution is compared to SCETlib+MCFM8, which provides predictions for $|y_{\gamma\gamma}|$ at NNLO+NNLL$'_\phi$ accuracy, derived by applying a resummation of the virtual corrections to the gluon form factor.
- The diphoton rapidity distribution is sensitive to the gluon distribution.
- Good agreement is observed over the full rapidity range.

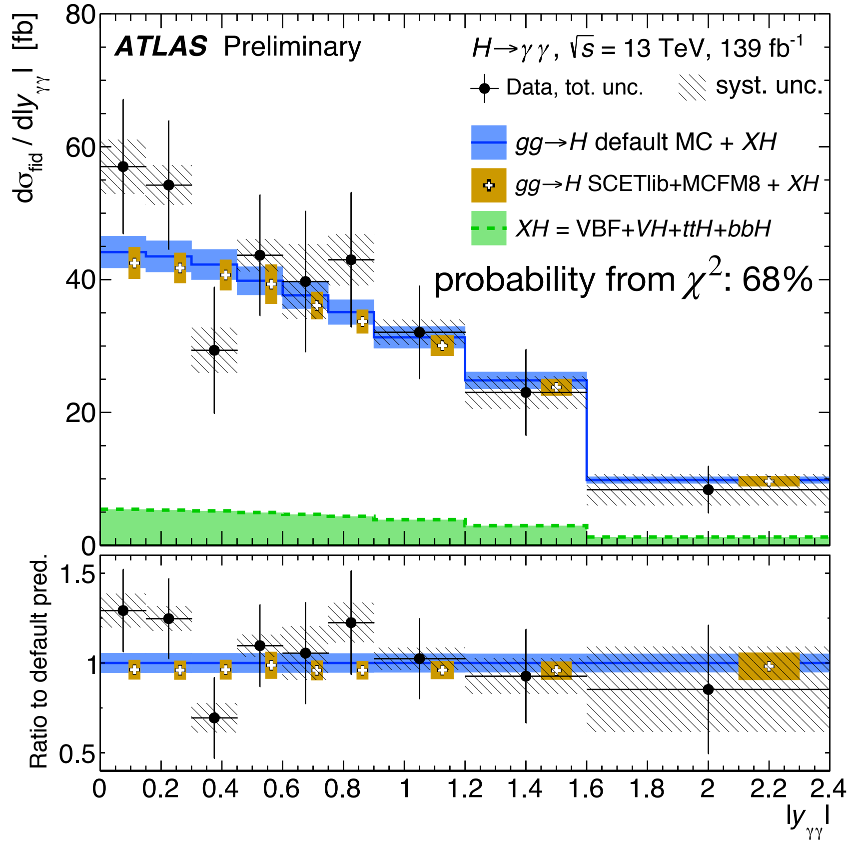

ATLAS-CONF-2019-029

$H \rightarrow \gamma\gamma$: differential and fiducial cross sections

- The inclusive fiducial cross section times the $H \rightarrow \gamma\gamma$ branching ratio is measured to be:

$$\sigma_{\mathrm{fid}} = 65.2 \pm 4.5\,(\mathrm{stat.}) \pm 5.6\,(\mathrm{syst.}) \pm 0.3\,(\mathrm{theo.})\ \mathrm{fb}$$

which is within one standard deviation of the default SM prediction of 63.6 ± 3.3 fb (arXiv: 1610.07922).

- The uncertainty of the fiducial measurement is equally affected by statistical and systematic uncertainties; when splitting in bins for the differential measurements, the statistical uncertainties dominate.

- The systematics associated to the signal extraction (background modelling and photon energy resolution) are typically larger than those on the correction factors, except for measurements with $N_{\mathrm{jets}} > 1$ where the impact of jet energy scale and resolution uncertainties on the correction factor become equally significant.

Source	Uncertainty (%)
Statistics	6.9
Signal extraction syst.	7.9
Photon energy scale & resolution	4.6
Background modelling (spurious signal)	6.4
Correction factor	2.6
Pile-up modelling	2.0
Photon identification efficiency	1.2
Photon isolation efficiency	1.1
Trigger efficiency	0.5
Theoretical modelling	0.5
Photon energy scale & resolution	0.1
Luminosity	1.7
Total	11.0

ATLAS-CONF-2019-029

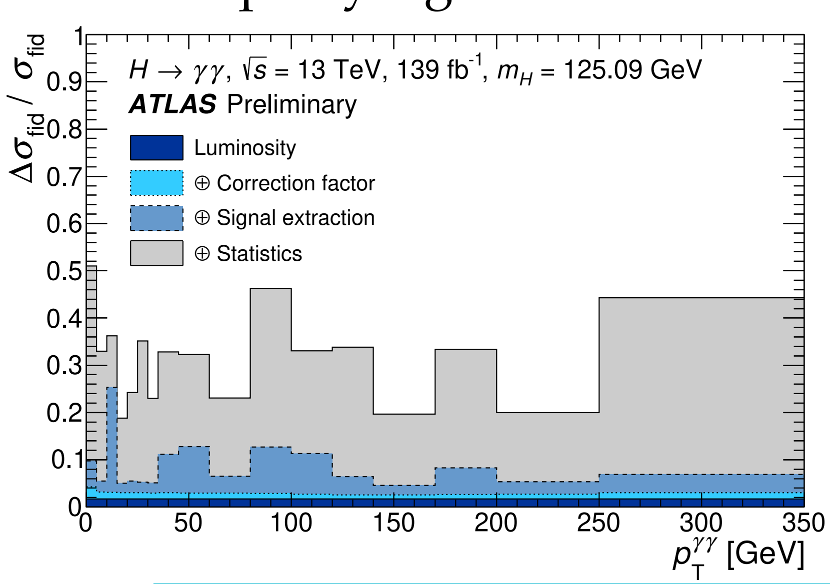

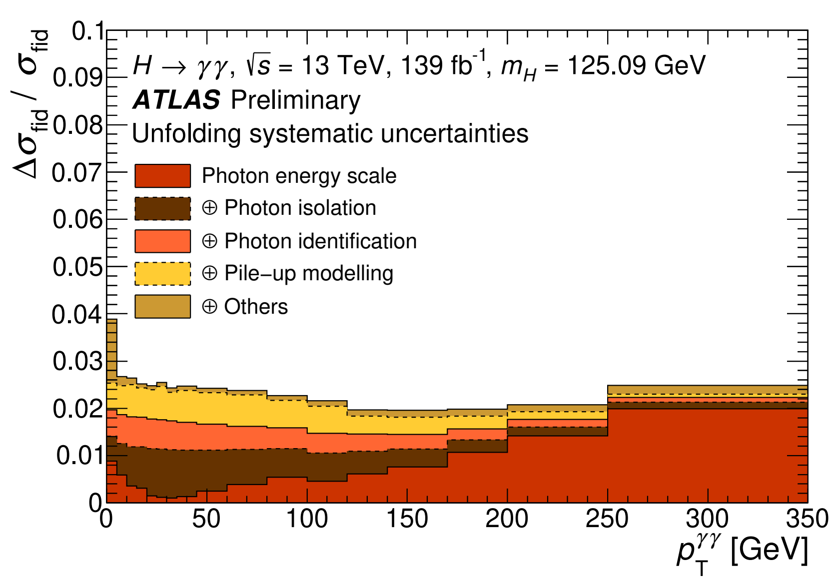

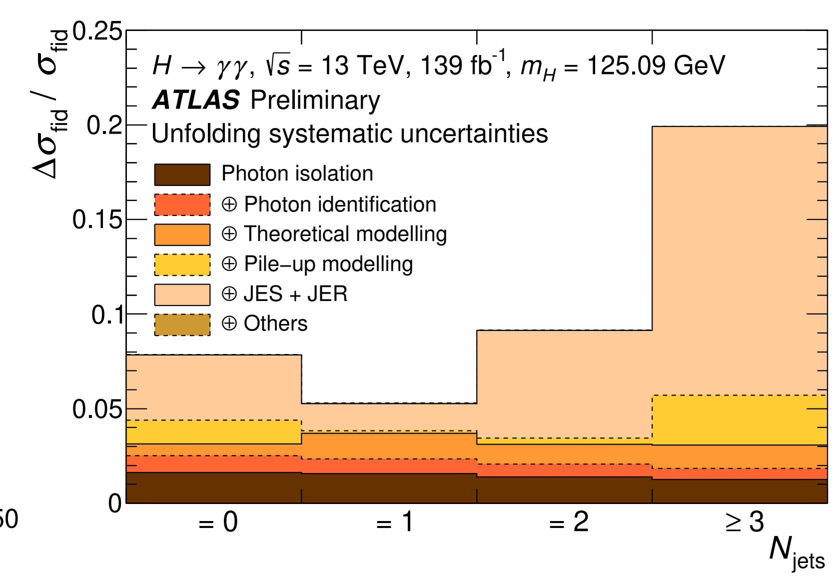

Anomalous Higgs-boson interactions through EFT

ATLAS-CONF-2019-029

- The impact of the $\bar{c}_g$ and $\tilde{c}_g$ coefficients is mainly on ggF, giving a large change in the overall cross-section normalisation; the $\tilde{c}_g$ coefficient also changes the shape of the $\Delta\phi_{jj}$ distribution.
- The impact of the $\bar{c}_{HW}$, $\bar{c}_{HB}$ and their CP-odd counterparts is mainly on VBF+VH production (large shape changes in all of the distributions).
- The $\Delta\phi_{jj}$ distribution discriminate between CP-even and CP-odd interactions in VBF production.

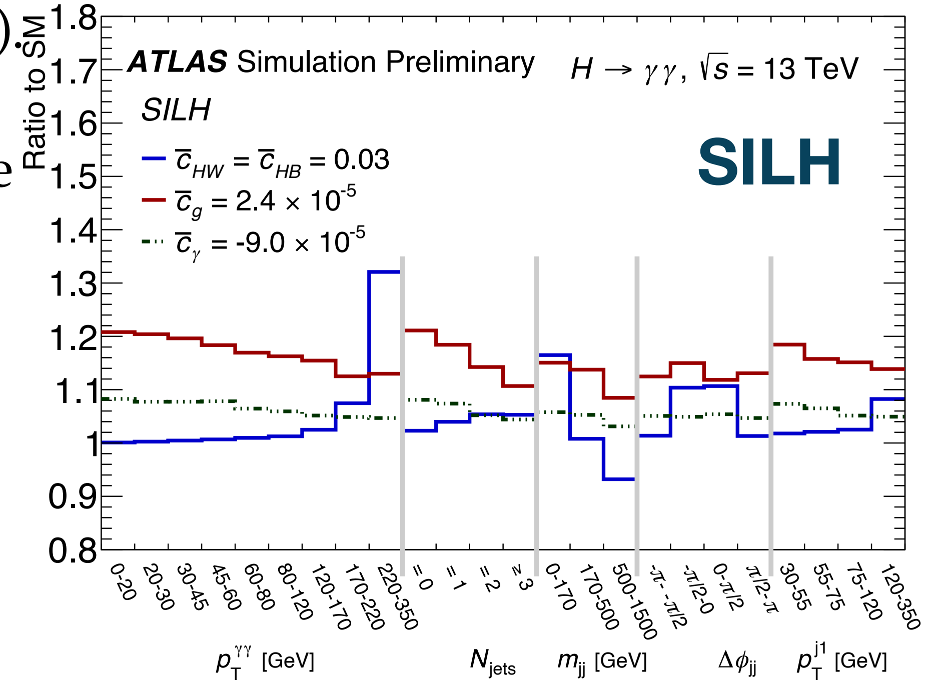

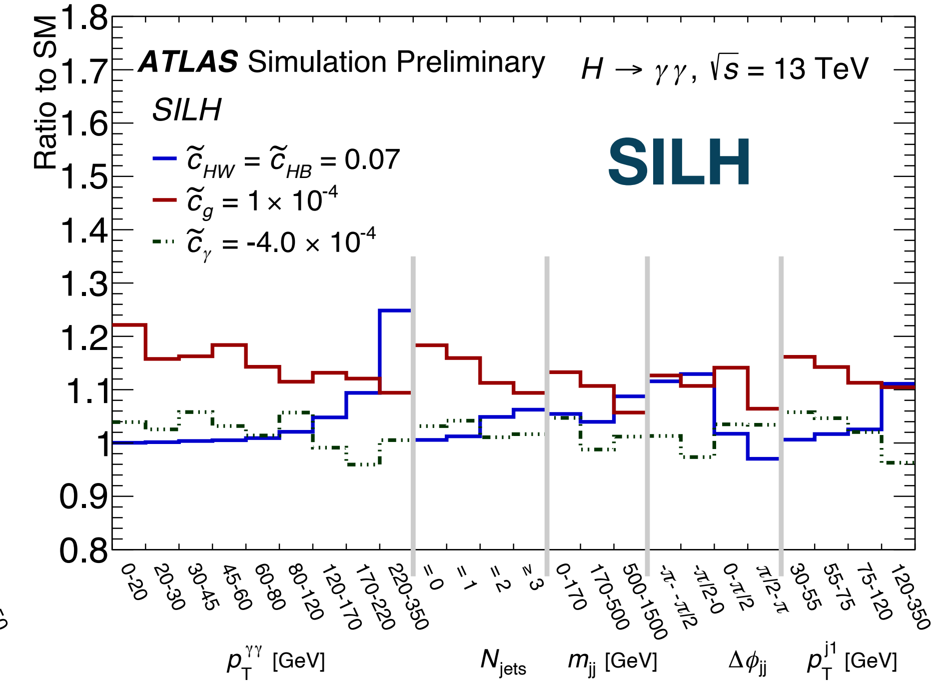

- The $\bar{C}_{HG}$ and $\tilde{C}_{HG}$ coefficients affect ggF production.
- $\bar{C}_{HB}$, $\bar{C}_{HW}$ and their CP-odd counterparts affect VBF+VH production; the main effect of $\bar{C}_{HB}$, $\bar{C}_{HW}$ and $\bar{C}_{HWB}$ is on the $H \to \gamma\gamma$ decay rate;
- The CP-odd coefficients exhibit sensitivity only to the $\Delta\phi_{jj}$ observable.

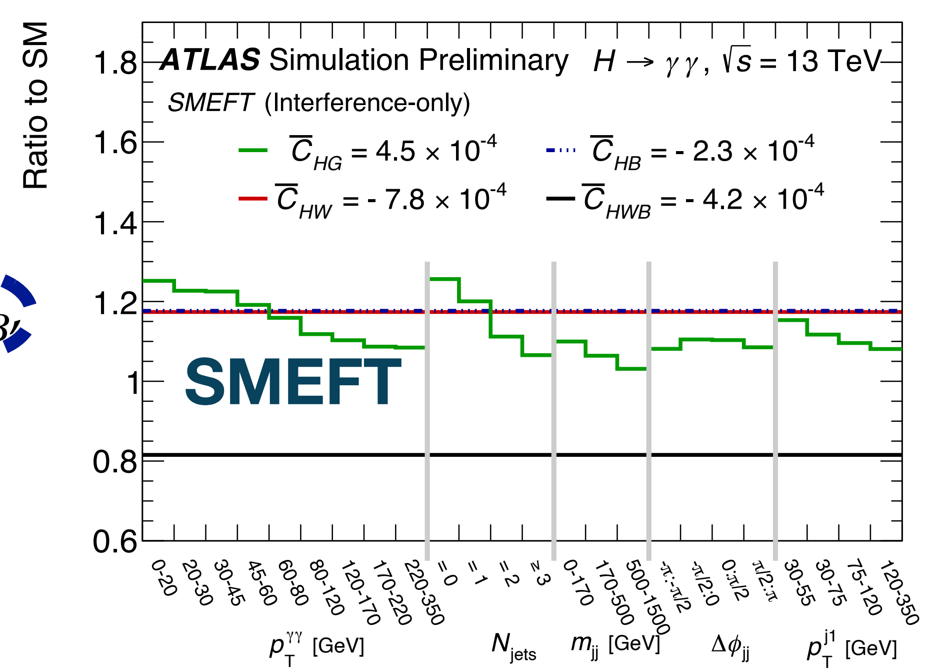

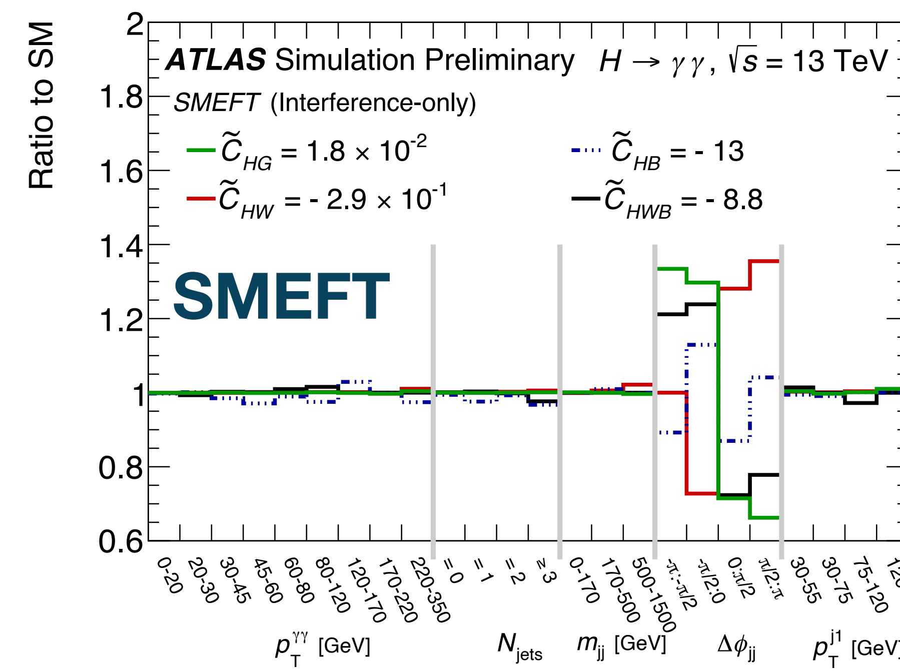

Anomalous Higgs-boson interactions through EFT

An effective field theory (EFT) approach can be used to interpret Higgs-boson interactions:

- additional CP-even and CP-odd interactions can change the event rates, the kinematic properties of the Higgs boson, etc.., from those predicted by the SM.

Wilson coefficients

$$\mathscr{L}_{EFT} = \mathscr{L}_{SM} + \sum_{i,D} \frac{c_i^{(D)}}{\Lambda^{D-4}} \mathscr{O}_i^{(D)}$$

- Dimension-6 operators are considered (dim-5 and dim-7 operators excluded -> lepton and baryon number conservation + dim-8 are neglected-> further suppressed by $1/\Lambda^2$).
- The differential $H \to \gamma\gamma$ cross sections are sensitive to operators that affect the Higgs-boson interactions with gauge bosons (5 differential distributions).

$$d(\sigma \times BR)/dx,\ x = p_T^{\gamma\gamma}, N_{jets}, p_T^{j1}, m_{jj}, \Delta\varphi_{jj}$$

$$\mathcal{L}_{\rm eff}^{\rm SILH} \supset \bar{c}_g O_g + \bar{c}_\gamma O_\gamma + \bar{c}_{HW} O_{HW} + \bar{c}_{HB} O_{HB} + \tilde{c}_g \tilde{O}_g + \tilde{c}_\gamma \tilde{O}_\gamma + \tilde{c}_{HW} \tilde{O}_{HW} + \tilde{c}_{HB} \tilde{O}_{HB}$$

$$\mathcal{L}_{\rm eff}^{\rm SMEFT} \supset \bar{C}_{HG} O'_g + \bar{C}_{HW} O'_{HW} + \bar{C}_{HB} O'_{HB} + \bar{C}_{HWB} O'_{HWB} + \tilde{C}_{HG} \tilde{O}'_g + \tilde{C}_{HW} \tilde{O}'_{HW} + \tilde{C}_{HB} \tilde{O}'_{HB} + \tilde{C}_{HWB} \tilde{O}'_{HWB}$$

- Two different EFT basis have been used:
  - ✦ the SILH basis of the Higgs Effective Lagrangian;
  - ✦ the Warsaw basis of the SMEFT Lagrangian.
- The contributions to the cross section can be separated into components for the SM, BSM and SM-BSM interference: $\sigma \propto |\mathcal{M}_{\rm EFT}|^2 = |\mathcal{M}_{\rm SM}|^2 + |\mathcal{M}_{\rm d6}|^2 + 2Re(\mathcal{M}_{\rm SM}^* \mathcal{M}_{\rm d6})$
- Limits on Wilson coefficients are set by building a likelihood function:

$$\mathcal{L} = \frac{1}{\sqrt{(2\pi)^k\,|C|}} \exp\left(-\frac{1}{2}\left(\vec{\sigma}_{\rm data} - \vec{\sigma}_{\rm pred}\right)^T C^{-1} \left(\vec{\sigma}_{\rm data} - \vec{\sigma}_{\rm pred}\right)\right)$$

  - $\vec{\sigma}_{data}$ and $\vec{\sigma}_{pred}$ are k-dimensional vectors from the measured and predicted differential cross sections of the five analysed observables;
  - $C = C_{stat} + C_{syst} + C_{theo}$ is the total covariance matrix.

Limits on the c-quark Yukawa coupling

Experimental evidence for Higgs boson couplings to the second generation quarks has not yet been found.

- Indirect approach: use the sensitivity of the Higgs boson $p_T^{\gamma\gamma}$ spectrum to the Yukawa couplings of the Higgs boson to the *c* (and *b-> not competitive with the direct observation).*
  - A modification in the coupling strength would impact:
    - ✦ the ggF ($gg \rightarrow H$) and quark-initiated production ($c\bar{c} \rightarrow H$), affecting both the normalisation and the shape of the $p_T^{\gamma\gamma}$ spectrum (impact on the acceptance found to be negligible);
    - ✦ the branching ratio for the $H \rightarrow \gamma\gamma$ decay (not used to set limits).

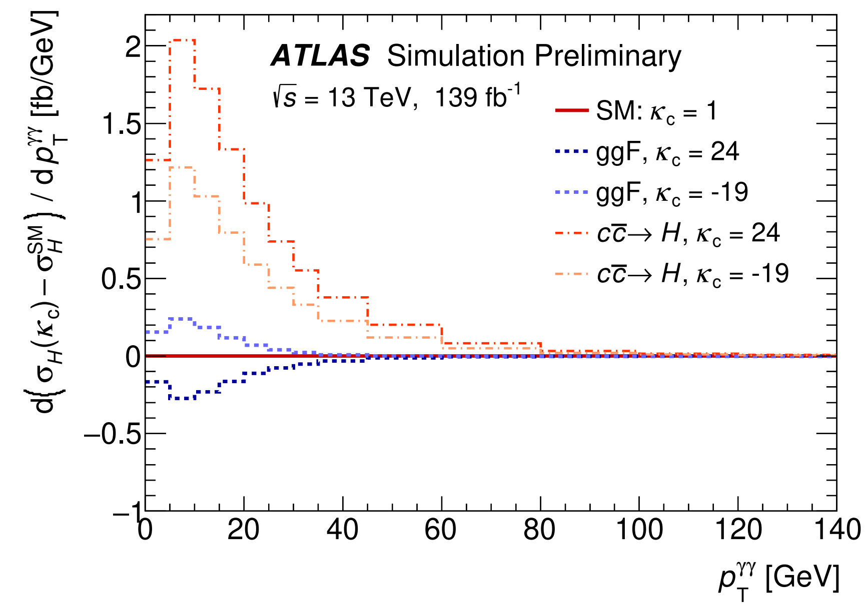

- The differential cross section is used in the range of $p_T^{\gamma\gamma}$ [0-140] GeV which is the region most sensitive to variations of κ_c.

- Limits on κ_c at 95% CL are $-19 < \kappa_c < 24$ (obs) - shape only.

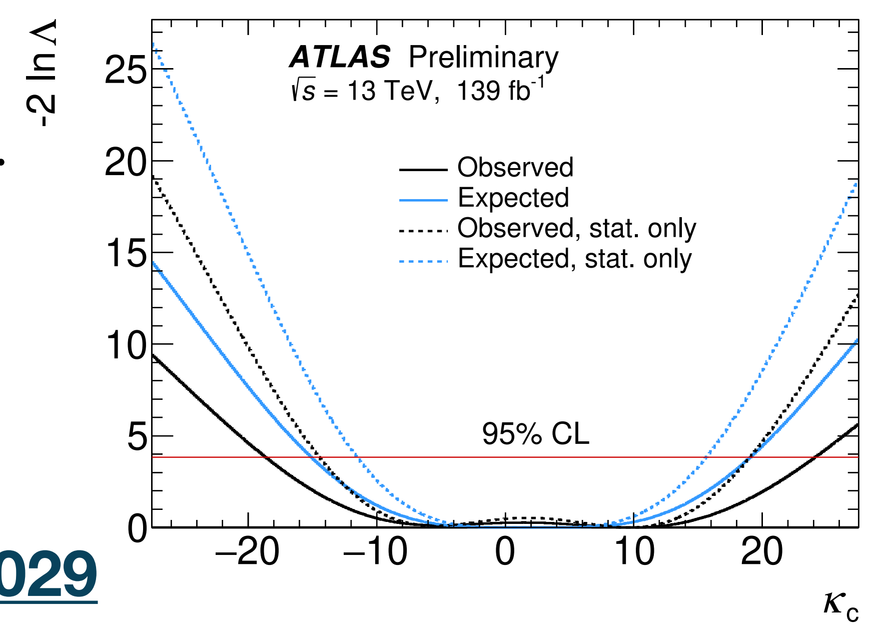

ATLAS-CONF-2019-029

$H \rightarrow \gamma\gamma$: inclusive cross sections

- ggF and VBF:
  - ✦ statistical ≈ systematic uncertainty;
  - ✦ largest systematics:
    - ggF: background modelling (4.1%),
    - VBF: signal modelling (10%).
- Given the large observed correlation between the measurements of WH and ZH cross-sections, a total cross-section for the WH and ZH production processes is measured: $\sigma_{VH,exp} = 4.53 \pm 0.12$ fb.
- SM compatibility of 5-POI fit: p-value = 3% (1.9 σ deviation).

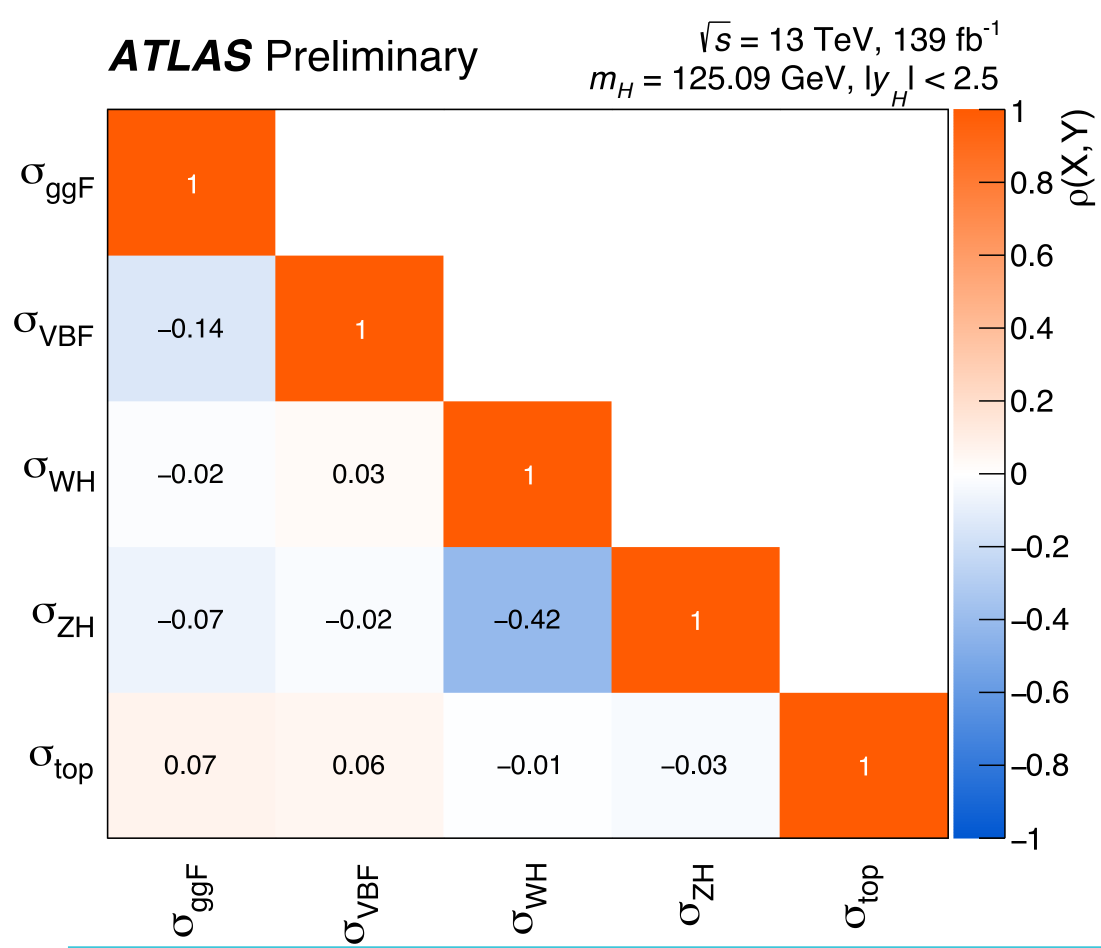

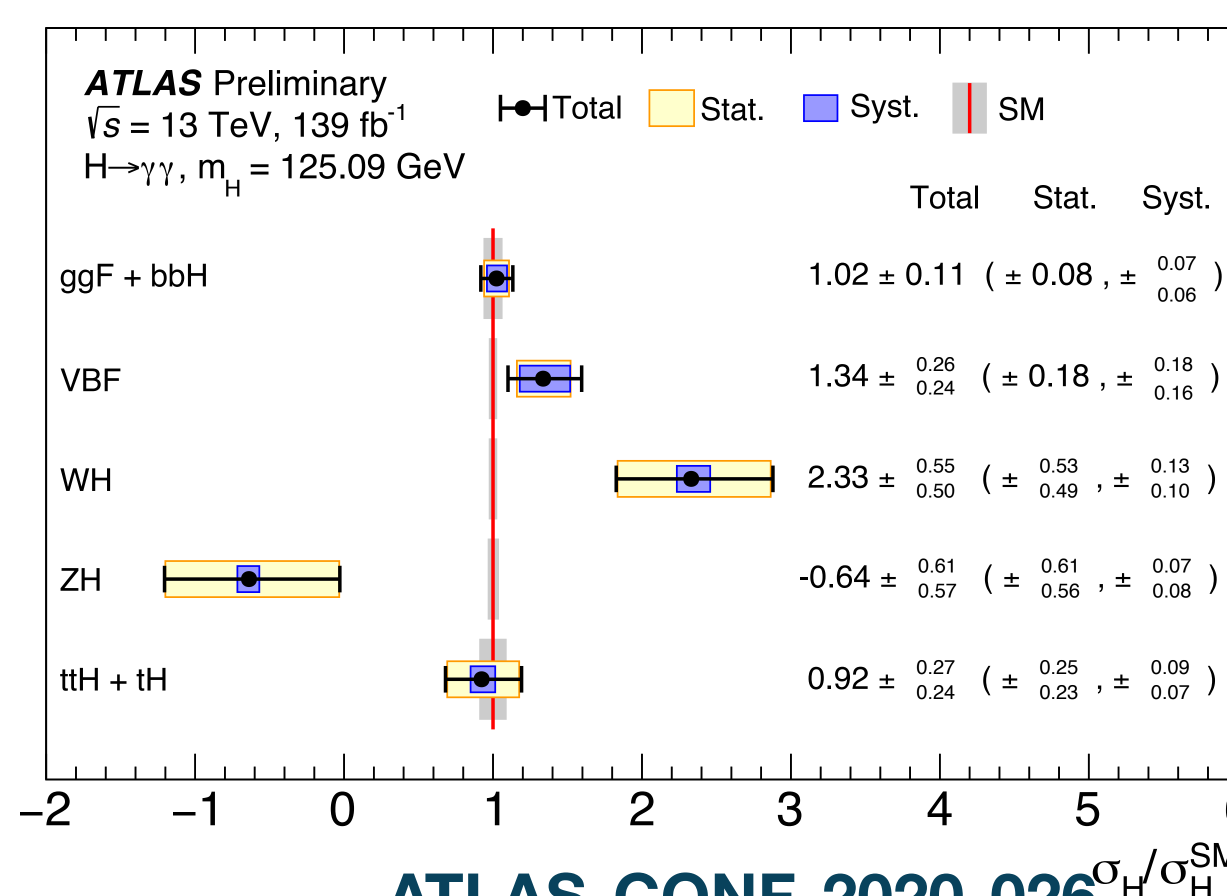

ATLAS-CONF-2020-026

$H \to \gamma\gamma$: inclusive cross sections

- ggF and VBF:
  - statistical ≈ systematic uncertainty;
  - largest systematics:
    - ggF: background modelling (4.1%),
    - VBF: signal modelling (10%).
- Given the large observed correlation between the measurements of WH and ZH cross-sections, a total cross-section for the WH and ZH production processes is measured: $\sigma_{VH,exp} = 4.53 \pm 0.12$ fb.
- SM compatibility of 5-POI fit: p-value = 3% (1.9 σ deviation).

	ggF+ $b\bar{b}H$	VBF	WH	ZH	$t\bar{t}H + tH$
Uncertainty source	$\Delta\sigma[\%]$	$\Delta\sigma[\%]$	$\Delta\sigma[\%]$	$\Delta\sigma[\%]$	$\Delta\sigma[\%]$
Underlying Event and Parton Shower (UEPS)	±2.3	±10	< ±1	±9.6	±3.5
Modeling of Heavy Flavor Jets in non-$t\bar{t}H$ Processes	< ±1	< ±1	< ±1	< ±1	±1.3
Higher-Order QCD Terms (QCD)	±1.6	< ±1	< ±1	±1.9	< ±1
Parton Distribution Function and α_S Scale (PDF+α_S)	< ±1	±1.1	< ±1	±1.9	< ±1
Photon Energy Resolution (PER)	±2.9	±2.4	±2.0	±1.3	±4.9
Photon Energy Scale (PES)	< ±1	< ±1	< ±1	±3.4	±2.2
Jet/$E_{\mathrm{T}}^{\mathrm{miss}}$	±1.6	±5.5	±1.2	±4.0	±3.0
Photon Efficiency	±2.5	±2.3	±2.4	±1.4	±2.4
Background Modeling	±4.1	±4.7	±2.8	±18	±2.4
Flavor Tagging	< ±1	< ±1	< ±1	< ±1	< ±1
Leptons	< ±1	< ±1	< ±1	< ±1	< ±1
Pileup	±1.8	±2.7	±2.1	±3.8	±1.1
Luminosity and Trigger	±2.1	±2.1	±2.3	±1.1	±2.3
Higgs Boson Mass	< ±1	< ±1	< ±1	±3.7	±1.9

ATLAS-CONF-2020-026

$H \to \gamma\gamma$: STXS cross sections

Training variables used for the BDTs

STXS regions	Multi-class BDT	STXS regions	Binary BDT
$gg \to H$	di-photon p_T and absolute rapidity; di-jet p_T, mass, Δy, $\Delta\phi$, $\Delta\eta$ between the 2 jets; p_T, mass of $\gamma\gamma + j$ and $\gamma\gamma + jj$, Δy, $\Delta\phi$ between $\gamma\gamma$ and jj, minimum ΔR between jets and photons, mass of the sum of all jets; di-lepton p_T, di-e or di-μ mass, E_T^{miss}, p_T of lepton + E_T^{miss}; p_T, η, ϕ, mass of top candidates; Number of jets, barrel jets ($\lvert\eta\rvert < 2.5$), b-jets and leptons; leading jet p_T, sum p_T of all jets $\sum E^T$, E_T^{miss} significance; Average interaction per crossing, number of primary vertices	individual STXS regions from $gg \to H$ or $qq' \to Hqq'$	Multi-class BDT variables, and $\Delta\phi$, $\Delta\eta$ between the 2 photons ($\Delta\phi_{\gamma\gamma}$, $\Delta\eta_{\gamma\gamma}$); Number of electrons and muons; E_T^{miss}, $\sum E^T$, E_T^{miss} significance, and E_T^{miss} azimuthal angle computed from hardest vertex; $\gamma\gamma$ p_T projected to its thrust axis ($p_{Tt}^{\gamma\gamma}$); Half difference between di-photon η and sum η of leading 2 jets (η^{Zepp}); $\phi^*_{\gamma\gamma} = \tan(\frac{\pi - \lvert\Delta\phi_{\gamma\gamma}\rvert}{2})\sqrt{1-\tanh^2(\frac{\Delta\eta_{\gamma\gamma}}{2})}$ $\cos\theta^*_{\gamma\gamma} = \lvert\frac{(E^{\gamma_1}+p_z^{\gamma_1})\cdot(E^{\gamma_2}-p_z^{\gamma_2})-(E^{\gamma_1}-p_z^{\gamma_1})\cdot(E^{\gamma_2}+p_z^{\gamma_2})}{m_{\gamma\gamma}+\sqrt{(m_{\gamma\gamma}^2+(p_T^{\gamma\gamma})^2)}}\rvert$
$qq' \to Hqq'$			
$qq \to H\ell\nu$		WH STXS regions combined	$p_T/m_{\gamma\gamma}$, η, ϕ of 2 leading photons; p_T, η, ϕ of 2 leading leptons; E_T^{miss}, E_T^{miss} significance, E_T^{miss} azimuthal angle; Whether or not the E_T^{miss} built from di-photon vertex is larger than that built from the hardest vertex by more than 30 GeV; di-lepton mass, and transverse mass of lepton + E_T^{miss}
$qq \to H\ell\ell$		ZH STXS regions combined	
$t\bar{t}H$		$t\bar{t}H$ STXS regions combined	p_T, η, ϕ of 2 leading photons; p_T, η, ϕ and B-tagging scores of 6 leading jets; E_T^{miss}, E_T^{miss} significance, E_T^{miss} azimuthal angle; Top reconstruction BDT scores
tH		tWH, $tHqb$	

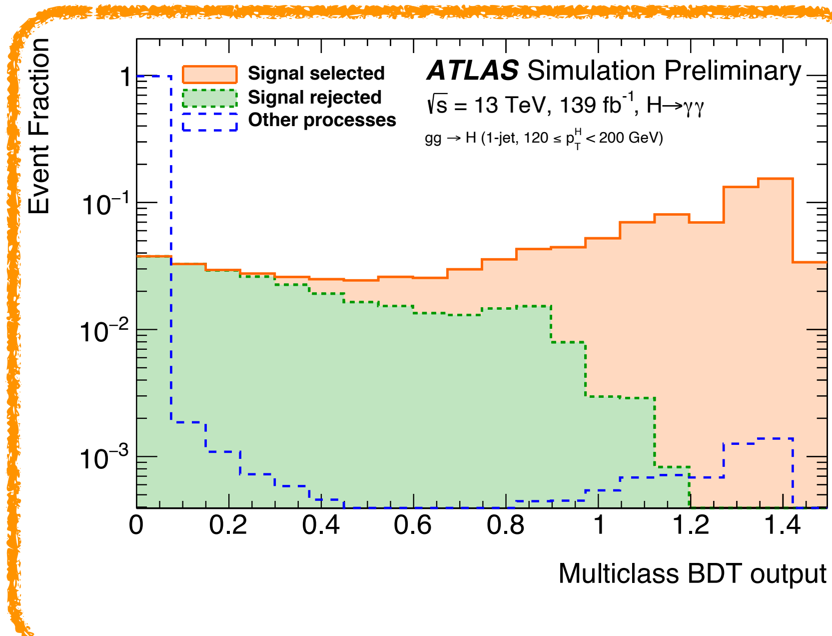

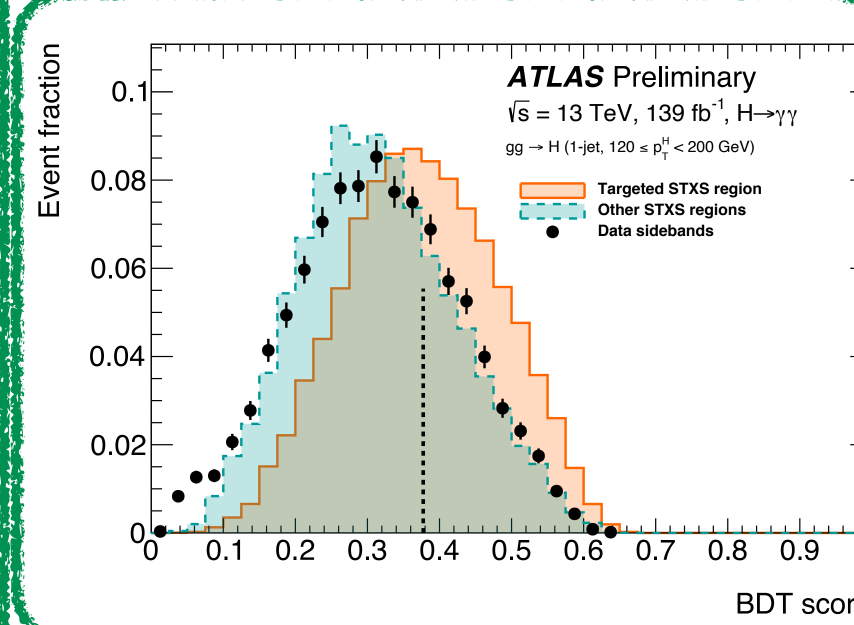

ATLAS-CONF-2020-026